Energy and Buildings 125 (2016) 86–98

Contents lists available at ScienceDirect

Energy and Buildings

journal homepage: www.elsevier.com/locate/enbuild

Nonlinear model predictive control for a heating and cooling system of a low-energy office building

Alexander Schirrer[a,*], Markus Brandstetter[a], Ines Leobner[b], Stefan Hauer[c], Martin Kozek[a]

[a] Institute of Mechanics and Mechatronics, Vienna University of Technology, Getreidemarkt 9, 1060 Vienna, Austria
[b] Institute for Energy Systems and Thermodynamics, Vienna University of Technology, Getreidemarkt 9, 1060 Vienna, Austria
[c] AIT Austrian Institute of Technology – ENERGY Department – Sustainable Buildings and Cities, Giefinggasse 2, 1210 Vienna, Austria

ARTICLE INFO

Article history:
Received 8 October 2014
Received in revised form 11 April 2016
Accepted 11 April 2016
Available online 24 April 2016

Keywords:
Nonlinear building control
Modular model predictive control
Robustness
Co-simulation
MPC
Mixed-integer optimization

ABSTRACT

Model predictive control (MPC) is highly suitable for building heating and cooling control because it exploits disturbance predictions, obeys constraints, and enables optimal building operation in terms of user comfort and energy efficiency. This work presents a highly efficient nonlinear modular MPC concept. It optimally controls both, heating and cooling activities in a low-energy office building simultaneously. Relevant system nonlinearities are considered through a nonlinear prediction model, an LTI MPC optimization step, and an efficient mixed-integer mapping to setpoint temperatures in the building. The involved optimization problems are efficiently solvable and enable realtime control, and the controller structure allows for retrofitting and can directly be incorporated into the existing building control infrastructure. A clear formulation of thermal user comfort and energy efficiency allows straightforward tuning. Excellent control performance and robustness are observed in detailed co-simulation studies, significantly outperforming a classical rule-based reference control law. Possible approaches to analyze robust stability of the controlled system are discussed and related to results of robust TS-fuzzy system analysis.

1. Introduction

1.1. Motivation and overview

The residential and commercial building sectors consume about 40% of the end use of energy world wide. The main part of about 75% accounts to heating, cooling, ventilation and preparation of hot water. Energy savings in the building sector thus contribute significantly to world-wide energy usage reduction. To secure the energy supply, the European Union declared that improving energy efficiency is the best way to guaranteeing energy security. A change of energy end use will thus play a major role in the reduction of greenhouse gases and pollution produced by the combustion of fossil fuels [1,2].

The control task in the present context is to provide satisfactory thermal user comfort at minimum energy consumption by a suitable building controller. A low-energy office building serves as basis for modeling, control design, and co-simulation-based validation.

Model Predictive Control (MPC) for building control has seen strongly increasing research interest in the last years: to tap the full energy-saving potential of actively controlled buildings (or enable active, optimal demand response in interaction with a smart energy grid), it is essential to exploit available predictions of the relevant disturbance effects (such as weather, solar radiation, occupancy, time-varying grid limitations, or dynamic pricing of grid energy). Also, system constraints typically have to be obeyed (e.g. limits on heat flow and temperature variation). These issues are optimally addressed by MPC which employs predictions of the future states of the system over a suitable horizon and optimizes, at each sampling instant, a sequence of control signal values so that a predefined objective is minimized while obeying the considered constraints. First experiments indicate a high energy saving potential for building systems that can be realized by using MPC instead of classical controllers such as Rule-Based Control (RBC) [3].

As outlined in [4], most building MPCs utilize linear time-invariant (LTI) prediction models of the building thermal behaviour. The resulting optimization problems (typically linear or convex

* Corresponding author.
E-mail addresses: alexander.schirrer@tuwien.ac.at (A. Schirrer), brandst.markus@gmx.at (M. Brandstetter), ines.leobner@tuwien.ac.at (I. Leobner), stefan.hauer@ait.ac.at (S. Hauer), martin.kozek@tuwien.ac.at (M. Kozek).

http://dx.doi.org/10.1016/j.enbuild.2016.04.029
0378-7788/

quadratic programs) are efficiently solvable, and various efforts have been made to extend these controllers' performance, robustness, and applicability. The resulting control input signals are often intermediate quantities (such as heat flows) that still need to be realized in the building services control system, for example via hierarchic or cascaded control schemes [5]. However, modern low-energy buildings often rely on energy supply services involving switched aggregates (e.g. heat pumps) or on/off-valves to distribute a centrally supplied feed flow to numerous building zones. Considering these nonlinearities correctly in optimization-based control allows to tap the full energy-saving potential of such building systems. The resulting hybrid system dynamics usually require high effort to solve optimal control problems; directly considering these effects via MPC typically generates mixed-integer optimization problems which quickly become untractable for real-time optimization when model complexity increases.

These aspects clearly show the need for an efficient MPC concept that addresses the relevant nonlinearities and fulfills realtime and retrofitting requirements. The modular MPC concept proposed in this work will be designed to fulfill these requirements.

1.2. Building model and nonlinearities

To model the building dynamics for MPC, a balanced complexity trade-off has to be found: the model has to be simple enough to be solved in an adequate amount of time but complex enough to reproduce the dynamics of the real building with sufficient accuracy. The modeling strategy is important, since obtaining the building model can be a time-demanding process, and it is crucial for the success of MPC [4]. A detailed discussion on advantages and disadvantages of different modeling strategies is given in [6]. To model the thermal building and building services behaviour, a common classification of the model type is

- black-box modeling as in [7–10],
- grey-box modeling with parameter identification as in [3,11–13], or
- white-box modeling as in [14,15].

Since for most new buildings extensive plan data are at hand, a white box modeling approach is chosen here. The model offers physical insight and reduces the need for on-site identification procedures. Difficulties of the identification process related to the persistent excitation property and the closed-loop nature of the model can be avoided [6,12].

Special care in modeling is required to adequately address the nonlinear and switching behavior of the building and the heating, ventilation and air conditioning (HVAC) system. Building models with nonlinear elements have been utilized in existing works: in [15], the state-space model is bilinear, taking into account the reduction of the solar radiation by pitching of window blinds. A static nonlinearity is compensated in [13] between the heat flux of the radiators and the temperature difference between inlet water temperature and zone temperature. Smooth nonlinear complex systems comprised of a set of local linear models are identified in [10]. A nonlinear model is the basis of the MPC in [14] where a chilling system is presented. However, the approach presented in the present work using a white-box nonlinear model is a novel idea.

Nonlinearities concerning switching parts of the building can be addressed in the MPC algorithm. These hybrid systems [16] are formulated for buildings in [14]. Nonlinear cost functions are formulated for example in [11,17].

1.3. Model predictive control in buildings

Building MPC has received considerable and sharply increasing research interest in the last years, see [18,4]. The authors of [18] discuss the trade-off between energy consumption and room comfort for occupants. In fact, MPC has two possibilities to improve the performance of buildings compared to RBC: Load shifting or active storage of energy, and optimizing the efficiency of the component mechanisms. Load control of the building mass is presented already in [19]. In that study the author points out that the saving potential is sensitive to weather conditions and occupancy schedules. The importance of occupancy information for MPC is presented more profoundly in [20].

The use of prediction data for MPC is crucial, but it is subject to uncertainties as mentioned in [18,4]. The uncertainty of predicted data (weather and internal gains) causes violations of the comfort criteria. This problem is taken into account in [21,22] by two concepts: Stochastic MPC and Randomized MPC, resulting in a robust controller for uncertain weather and internal gain predictions.

Several simulation studies concerning building MPC are performed e.g. in [17,22,23]. The authors in [12,13,24] perform simulation studies for intermediate heated buildings, defined by a change of the room reference temperature during off-hours. This is also considered here for the office building controlled in this paper.

Recent experimental results show the potential of MPC in buildings: An online full-scale implementation of an MPC for an HVAC system is presented in [11]. The results of the MPC are delivered as set points to the controllers of the lower control level. The energy consumption is reduced by up to 60% compared to RBC. In [14] an HVAC MPC for a chilling system is presented. The controller improved the coefficient of power (COP) by 19.1% when being implemented at the University of California, Merced campus, USA. Experiments using thermally activated building systems are presented in [3,7]. While in [7] only predictions of the outside temperatures are utilized, Ref. [3] performs the experiments with weather and occupancy predictions. In both articles the MPC is compared to RBC or similar control strategies. The authors state an energy saving potential of about 20%.

Most of the MPC consider either heating or cooling systems, those being capable to optimize both heating and cooling of a building ventilation system simultaneously can be found in [9,11,23]. Only the publications concerning the OptiControl project report simulations of cooling and heating thermally activated building systems (TABS), see [15,21,22].

1.4. Proposed modular MPC concept for building control

This paper presents a novel model predictive controller scheme for the heating and cooling system of a low-energy building using prediction data for weather and internal gains (occupancy, lights). A modular Model Predictive Control (MMPC) concept is devised that fulfills the following requirements: realtime capability, detailed modeling (16 states corresponding to 16 zone temperatures) of a nonlinear hybrid dynamic building system, and direct integrability into the existing building control system by providing TABS temperature setpoint trajectories. The MMPC exploits an available nonlinear prediction model, adjusts the temperatures and heat flows of the building system to optimize energy efficiency and thermal comfort based on a linear thermal model, and maps the resulting heat flows optimally to TABS setpoint trajectories via a reduced-complexity mixed-integer optimization step. This way, high control performance and robustness are obtained, computational effort is kept small so as to enable real-time control, and the concept is well-suited for retrofitting of existing building control systems.

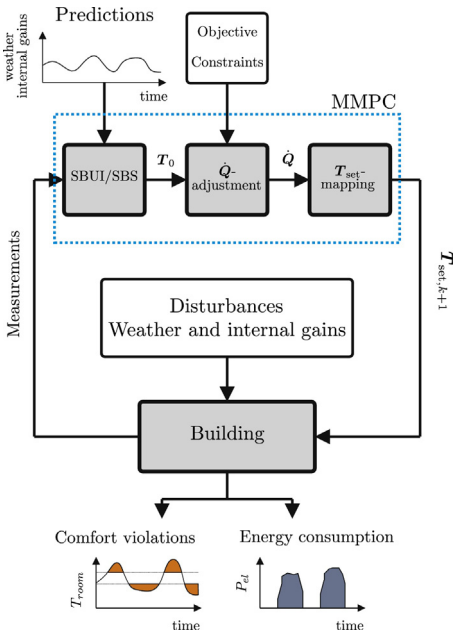

Fig. 1. Control scheme for MMPC, $\boldsymbol{T}_{set}$ are the set point temperature trajectories for the TABS, $\boldsymbol{T}_{set,k+1}$ the TABS set points for the next time step $k+1$, $\widetilde{\boldsymbol{T}}_0$ are the baseline trajectories, $\dot{\boldsymbol{Q}}$ are the trajectories of the heat flows to the TABS, T_{room} is the room temperature, P_{el} is the electric power consumption, SBUI/SBS is the simplified building and building services model.

The MMPC is structured as shown in Fig. 1. The control signal computed by the MMPC are finally the TABS temperature set points $\boldsymbol{T}_{set}$ which allow direct interfacing to the existing building's interface. The MMPC consists of 3 functional modules executed at each sampling step: first, the simplified nonlinear building and services model (SBUI/SBS) is simulated using predicted disturbances to provide a baseline prediction of temperatures $\boldsymbol{T}_0$ and heat flows $\dot{\boldsymbol{Q}}_0$ (module 1). Then, an LTI MPC problem is solved to adjust the heat flows ($\dot{\boldsymbol{Q}}$-adjustment, module 2) to optimize the control objectives and obey control constraints. Finally, the TABS setpoints are obtained by solving a mixed-integer optimization problem ($\boldsymbol{T}_{set}$-mapping, module 3). Module 3 realizes the optimized heat flows as closely as possible by the switching actuation behaviour caused by the switching-valve hydraulic distribution of the feed line into the TABS. This switching pattern is formulated as suitable TABS setpoint temperature signals and fed to the subsystem controllers present in the building. The modular concept enables the controller to approximate the globally nonlinear optimization problem well and to solve the decoupled subproblems efficiently. It is further shown that the MMPC is robust to significant prediction and model errors. For co-simulation studies a high-fidelity white-box

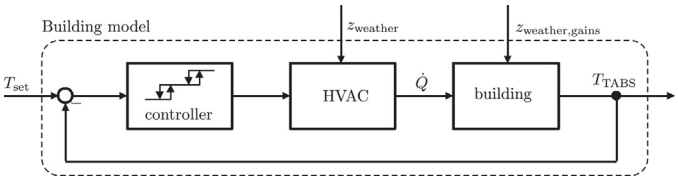

Fig. 3. Model structure of the building with the building services (basic automation and HVAC) and corresponding disturbances. Set point temperatures for the TABS are denoted by T_{set}, $\dot{Q}$ denotes the heat flows to the TABS, and T_{TABS} the actual TABS temperatures.

model, the complex building model and building services model (CBUI/CBS), is used to replace the real building in the control loop.

The remainder of this paper is structured as follows: Section 2 describes the system model, the control problem and the control goals, which lead to the proposed MMPC concept. Section 3 describes the MMPC in detail, followed by stability and robustness considerations discussed in Section 4. Finally, building model validation results and the results of detailed co-simulation studies demonstrate the high control performance and robustness in Section 5, followed by conclusions in Section 6.

2. System model and problem statement

In the following, the investigated building, the nonlinear building modeling, and the model structures utilized for control design and validation are outlined. In this context, the control goals are then formulated, and specific difficulties in the control problem highlighted, leading to the proposed modular MPC concept as an efficient solution.

2.1. Building description

The investigated building (ENERGYbase, see Fig. 2) is a low-energy office building constructed according to the passive house standard and is located in Vienna, Austria [25]. The ENERGYbase is a 5-level office building and offers approximately $A = 5000\text{m}^2$ office space. Its total annual electric energy demand for all HVAC components is approximately $E = 25\,\text{kWh/m}^2$. The building heating/cooling system consists of a solar thermal system supporting the two thermal heat pumps, supplied by two well pumps, to produce the necessary heat flows for the TABS.

2.2. Building model structures

An overview of the system parts modeled in the complex (CBUI/CBS) and simplified building models (SBUI/SBS) is given in Fig. 3. The models each consist of three major parts: the HVAC system, the building thermal dynamics itself, both described in more detail below, and the control logics used to control HVAC

Fig. 2. ENERGYbase low-energy office building in Vienna, Austria.

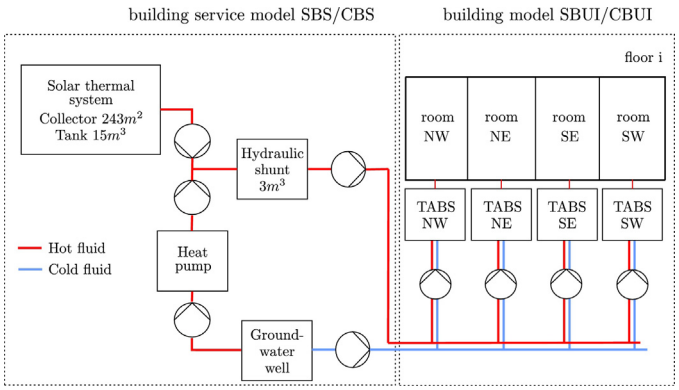

Fig. 4. Heating and cooling system of the building. Parts of the simple/complex building services model (SBS/CBS) and the simple/complex building model (SBUI/CBUI). Floor i represents one of the 5 floors of the building.

devices based on set point and measured temperatures. The nonlinear and switching behavior of the building model as mentioned in Section 1.2 mainly comes from the discontinuous subsystem controllers (e.g. thermostats) used to control the heating and cooling system based on the actual TABS temperatures T_{TABS} and the TABS set point temperatures T_{set}. Other nonlinearities are system components with nonlinear characteristics over the operating range (heat pump, solar collector, pumps) and devices controlled by time or ambient conditions such as air conditioning (AC) systems or radiation-controlled window blinds.

The modeled heating and cooling system is shown in Fig. 4 which illustrates the structure of the HVAC system used for room conditioning and the structure of the building model. Heating is provided by two sources: a solar thermal system and two heat pumps supplied with ground water. Cooling is provided directly from the ground water source. The energy for heating and cooling is injected directly into the concrete cores of the TABS via four lines in each floor.

Two different models are developed in Modelica, see [26], serving as a basis for the MPC controller and its validation: SBUI/SBS and CBUI/CBS. Either can be split into the building model (SBUI/CBUI) and the building services model (SBS/CBS), see Fig. 4. CBUI/CBS is a high-fidelity model validated with measurement data which has been generated to simulate different configuration variants of the building equipment and the energy consumption as accurately as possible. It is used to validate the MMPC in co-simulation studies. CBUI/CBS serves as basis for the simplified variant SBUI/SBS. The SBUI/SBS model provides the predicted baseline trajectories $\widetilde{\boldsymbol{T}}_0$ (MMPC module 1) and needs real-time capability (for a later real-time implementation), which is not required for CBUI/CBS. With constant coefficients and constant fluid mass flows, the thermal building dynamics of the SBUI model part is linear and time-invariant. Further model reduction yields an efficient LTI prediction model for the LTI MPC step (MMPC module 2). This prediction model fully accounts for cross-coupling and for the multivariable nature of the thermal dynamics.

2.2.1. Nonlinear complex model (CBUI/CBS)

The CBUI/CBS model is modeled following the German standard VDI 6020, known as “Beuken-Model” [27] by Modelica’s physical acausal modeling approach. This approach represents thermal zones by a resistances and capacitances network (RC-network) resulting in a good balance between model simplicity and model quality. The abstracted building model of the ENERGYbase is divided into different levels of detail: one floor (RC-network) as well as a single thermal zone are shown in Fig. 5.

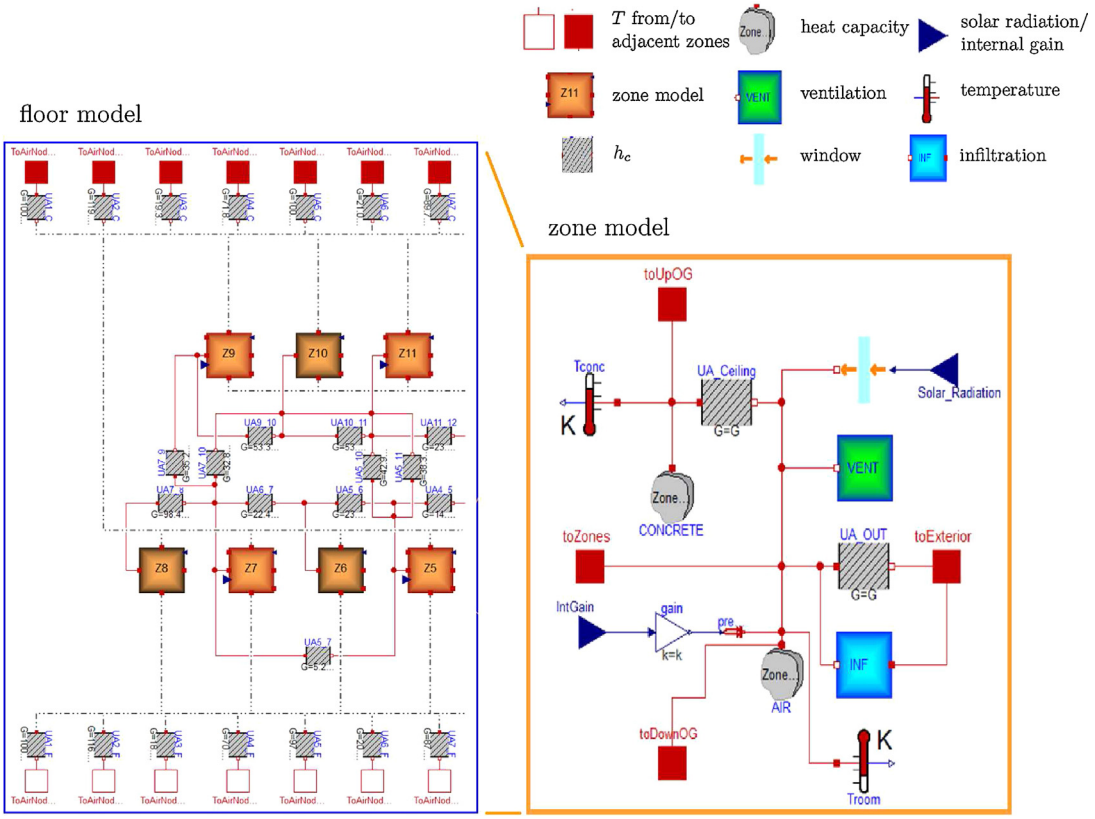

Fig. 5. Floor model and thermal zone model of the Complex Building Model (CBUI), with T the air or TABS temperature, h_c the thermal conductance, modeled in Modelica, compare [26].

In order to create the CBS model all necessary HVAC components as shown in Fig. 4 are modeled individually and assembled. Automated solar blinds affecting the solar radiation to the rooms are considered as well.

2.2.2. Nonlinear simplified model (SBUI/SBS)

Based on plan data and simulation results of CBUI/CBS a white-box simplified model SBUI/SBS is generated. The number of thermal zones in each floor is reduced to 4 aggregated zones corresponding to the sectors of the hydraulic system (NW north west, NE north east, SE south east, and SW south west). Instead of a physical bond-graph-based approach, SBUI/SBS is created based on energy balances and causal energy flows. The calculation time of the simplified model in comparison to the complex model is reduced by a factor of $f = 300$, and it delivers 2 day prediction data within $t = 5$ s computation time,[1] which fulfills the requirements for a real-time application.

SBUI/SBS generates the baseline trajectory $\widetilde{\boldsymbol{T}}_{0,k} = [\boldsymbol{T}_{0,\mathrm{TABS},k}, \boldsymbol{T}_{0,\mathrm{room},k}, P_{\mathrm{el},0,k}, \dot{\boldsymbol{Q}}_{0,k}]$ consisting of the baseline values of the room and the TABS temperatures, the consumed total electric power and the heat flow to the TABS at time step k,

$$\widetilde{\boldsymbol{T}}_{0,k+1} = \boldsymbol{f}_{\mathrm{SBUI/SBS}}(\widetilde{\boldsymbol{T}}_{0,k}, \boldsymbol{z}_{\mathrm{weather,gains},k}), \tag{1}$$

with $\boldsymbol{z}_{\mathrm{weather,gains},k}$ the predicted trajectories of weather and internal gain signals, and the model equation update function $\boldsymbol{f}_{\mathrm{SBUI/SBS}}$, describing the behavior of the building. Modeling and calculation are performed with the simulation environment Dymola.

2.2.3. Linearized thermal state-space model

The thermal dynamics of the building are obtained by linearization and model reduction of the building model SBUI. The state-space matrices are invariant with respect to time or states (temperatures), hence an LTI model is obtained:

$$\begin{aligned} \boldsymbol{x}_{k+1} &= \boldsymbol{A}\boldsymbol{x}_k + [\boldsymbol{B}, -\boldsymbol{B}] \left.\begin{bmatrix} \dot{\boldsymbol{Q}}_{\mathrm{heat},k} \\ \dot{\boldsymbol{Q}}_{\mathrm{cool},k} \end{bmatrix}\right\} \boldsymbol{u}_k \\ \boldsymbol{y}_k &= \boldsymbol{C}\boldsymbol{x}_k + [\boldsymbol{D}, -\boldsymbol{D}] \left.\begin{bmatrix} \dot{\boldsymbol{Q}}_{\mathrm{heat},k} \\ \dot{\boldsymbol{Q}}_{\mathrm{cool},k} \end{bmatrix}\right\} \boldsymbol{u}_k, \end{aligned} \tag{2}$$

with the state matrix $\boldsymbol{A}$, the input matrix $\boldsymbol{B}$, the output matrix $\boldsymbol{C}$, and the feed-through matrix $\boldsymbol{D}$. Input vector $\boldsymbol{u}_k$ consists of the heat flows, which are decomposed into heating flows $\dot{\boldsymbol{Q}}_{\mathrm{heat},k}$ and cooling flows $\dot{\boldsymbol{Q}}_{\mathrm{cool},k}$ at time step k. The state vector $\boldsymbol{x}_k$ contains the room temperatures $\boldsymbol{T}_{\mathrm{room},k}$ and the TABS temperatures $\boldsymbol{T}_{\mathrm{TABS},k}$. Output vector $\boldsymbol{y}_k$ additionally contains the electric power consumption $P_{\mathrm{el},k}$, as shown in Fig. 6.

To control heating and cooling, $\boldsymbol{B}$ and $\boldsymbol{D}$ have to be augmented, using $-\boldsymbol{B}$ and $-\boldsymbol{D}$ for the cooling flow, so that $\dot{\boldsymbol{Q}}_{\mathrm{cool},k} > 0$ holds. The feed-through matrix $\boldsymbol{D}$ occurs in (2) because the input heat flow immediately requires electric power. Due to the structure of the MMPC the disturbances (weather and internal gains) do not enter the LTI state-space model. The state-space model has heat flows as inputs as in e.g. [12].

2.2.4. Building zone distribution and model reduction

Index $f \in \{$ F0, F1, F2, F3, F4$\}$ denotes one of the 5 levels of the building. For example, the heating/cooling flows are denoted by $\dot{\boldsymbol{Q}}_{\mathrm{heat/cool},k} = \left[\dot{\boldsymbol{Q}}_{\mathrm{F0},k}^{\mathrm{T}}, \dot{\boldsymbol{Q}}_{\mathrm{F1},k}^{\mathrm{T}}, \dot{\boldsymbol{Q}}_{\mathrm{F2},k}^{\mathrm{T}}, \dot{\boldsymbol{Q}}_{\mathrm{F3},k}^{\mathrm{T}}, \dot{\boldsymbol{Q}}_{\mathrm{F4},k}^{\mathrm{T}}\right]^{\mathrm{T}}$. Moreover, floors F0, …, F4 of the building are each split up into 4 zones (NW, NE, SE, SW). Level F0 is split up only into 2 zones (west W and east E). Heat flows can be provided to all zones in each level, except for the ground floor, where heat flows are only provided to the western zone. However, due to similar behavior of certain areas, the state space model is reduced to 16 states, 17 outputs and 16 input variables by suitable transformation matrices. The northern and the southern zones and the second and third floors are accumulated each into one zone, resulting in the zones $j \in \{$N, S$\}$ and the floors $f \in \{$ F0, F1, F23, F4$\}$. The chosen fundamental sampling time of $T_s = 15$ min of the MMPC is chosen equal to the existing RBC sampling time. The reduced state-space model is being utilized as prediction model for the LTI MPC (module 2).

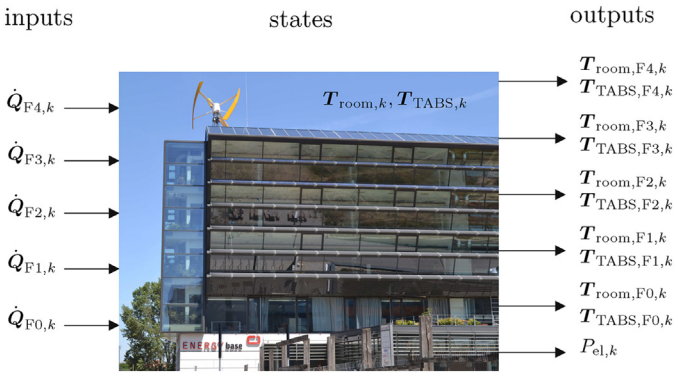

Fig. 6. Scheme of the thermal LTI state-space model of the building, with the room and TABS temperatures $\boldsymbol{T}_{\mathrm{room},f,k}$, $\boldsymbol{T}_{\mathrm{TABS},f,k}$, the heat flow to the TABS $\dot{\boldsymbol{Q}}_{f,k}$ of floor $f \in \{$ F0, F1, F2, F3, F4$\}$ at time step k. Inputs, outputs, and states are understood as deviations from the respective linearization values.

2.3. Control goals

The control goals for the presented MMPC are:

- produce stable closed-loop dynamics,
- minimize energy consumption or cost, and
- fulfill temperature band requirements for thermal user room comfort during office hours.
- Moreover, given system constraints (heat flow limits, limited electric power drawn from the grid, exploitation of local thermal storage components) need to be obeyed.

The control goal formulations (energy prices, comfort temperature bands) are considered as generally time-varying. Doing so allows to flexibly integrate the controlled building as an active participant in smart energy grids and to consider dynamic grid constraints [28]. Also, the temperature comfort band requirements only need to be fulfilled during office hours, opening an energy-saving potential at night. In Ref. [24], the temperature band is widened during off-hours, however, in the present work temperature constraints are entirely dropped at these times to maximize the attainable energy-saving potential.

One choice of performance criteria that have been utilized in building control are the use of electric energy and the peak energy consumption, see for example [3,11,13]. The authors in [14] directly formulate the electric bill in their cost function. Low-level controllers for air control often include comfort indices such as the predictive mean vote (PMV) or the ASHRAE standard in the cost function to optimize humidity and temperature in the controlled zones [8,9,29].

In this paper, the energy consumption is formulated as linear minimization objective (as in [13]), and the room temperatures are to be kept inside a given thermal comfort band.

[1] Obtained with an Intel Core i7-4600 CPU @ 2.10/2.7 GHz.

2.4. Nomenclature

The utilized notation is clarified using the room temperature as an example. The trajectories of all zones (N, S) and floors (F0, F1, F23, F4) of the building over the whole prediction horizon N_p are represented in $\boldsymbol{T}_\mathrm{room} = [\boldsymbol{T}_{\mathrm{room},0}, \ldots, \boldsymbol{T}_{\mathrm{room},N_\mathrm{p}-1}]$. Each quantity $\boldsymbol{T}_{\mathrm{room},k} = [\boldsymbol{T}^\mathrm{T}_{\mathrm{room,F0},k}, \ldots, \boldsymbol{T}^\mathrm{T}_{\mathrm{room,F4},k}]^\mathrm{T}$ denotes the room temperatures of all zones and floors at time step k. $\boldsymbol{T}_{\mathrm{room},f,k} = [T_{\mathrm{room},f,\mathrm{N},k}, T_{\mathrm{room},f,\mathrm{S},k}]^\mathrm{T}$ contains the room temperatures of all zones in floor f at time step k. $T_{\mathrm{room},f,j,k}$ is the room temperature of floor f and zone j at time step k, for example $T_{\mathrm{room,F0,S},5}$.

This nomenclature is used in the following sections for all trajectories of vector signals. For trajectories of scalar signals such as the electric power $\boldsymbol{P}_\mathrm{el}$, the symbol $P_{\mathrm{el},k}$ denotes the electric power at time step k.

3. Control design

The MMPC concept is developed in the following as an efficient means to address the set of requirements and control goals outlined above. The MMPC's three modules and their interplay are described and the involved optimization problems are defined. Extensions to utilizing solar heating storage as a cost-free heating source as well as move blocking are outlined. A discussion on ways to verify robust stability with the proposed control concept follows in Section 4.

3.1. Model predictive control for buildings: basic algorithm

For a system of the form

$$\boldsymbol{x}_{k+1} = \boldsymbol{f}(\boldsymbol{u}_k, \boldsymbol{x}_k, \boldsymbol{z}_{\mathrm{weather,gains},k})$$

with input vector $\boldsymbol{u}_k$ and state vector $\boldsymbol{x}_k$, the generic discrete-time optimization problem of a building MPC for energy-efficient heating and cooling as utilized for the proposed MMPC is formulated as:

$$J(\boldsymbol{x}_k, \boldsymbol{u}_k) = \sum_{i=0}^{N_\mathrm{p}-1} l_{k+i}(\boldsymbol{x}_{k+i}, \boldsymbol{u}_{k+i}) + g(\boldsymbol{x}_{k+N_\mathrm{p}-1}, \boldsymbol{u}_{k+N_\mathrm{p}-1}) \tag{3}$$

$$\boldsymbol{u}_k^* = arg \min_{\boldsymbol{u}_{k\ldots k+N_\mathrm{p}-1}} J(\boldsymbol{x}_k, \boldsymbol{u}_k) \tag{4}$$

$$\text{s.t.} \quad \forall i = 0, \ldots, N_\mathrm{p} - 1 : \tag{5}$$

$$\boldsymbol{u}_{k+i} = \boldsymbol{0} \quad \text{if} \quad \eta_{k+i} = 0 \tag{6}$$

$$\bar{\boldsymbol{x}} = \boldsymbol{x}_\mathrm{ref} \tag{7}$$

$$\boldsymbol{x}_{k+i} \in \mathbb{X}_{k+i} \tag{8}$$

$$\boldsymbol{u}_{k+i} \in \mathbb{U}_{k+i} \tag{9}$$

$$\boldsymbol{x}_{k+i} = \boldsymbol{f}(\boldsymbol{u}_{k+i-1}, \boldsymbol{x}_{k+i-1}, \boldsymbol{z}_{\mathrm{weather,gains},k+i-1}) \tag{10}$$

with N_p the prediction horizon, $\boldsymbol{f}$ the system equation update function, the optimal solution for the inputs of the optimization problem $\boldsymbol{u}_k^*$, $\mathbb{X}$ the set of state constraints and $\mathbb{U}$ the set of input constraints at prediction step i. $\boldsymbol{x}_\mathrm{ref}$ denotes the reference for the time-averaged states (temperatures), and $\bar{\boldsymbol{x}} = (1)/(N_\mathrm{p}) \sum_{i=0}^{N_\mathrm{p}-1} \boldsymbol{x}_{k+i}$ denotes the time-averaged state (temperature) values. The heating/cooling variable is defined as $\eta_{k+i} = 1$ when heating/cooling of the building is allowed and zero otherwise. The stage costs l_{k+i} and the terminal costs g form the cost function J, which is minimized over the prediction horizon. The optimization problem respects the set of constraints on the inputs (9) and the set of constraints on the states as in (8). This optimization problem is solved at each sampling step and only the inputs of the next time step are fed to the system (receding horizon principle).

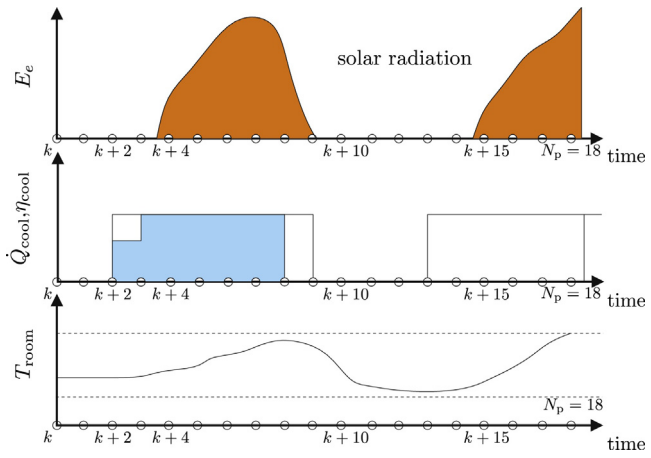

Fig. 7. Scheme of a building MPC behavior for one room in floor f, solar radiation $\boldsymbol{E}_\mathrm{e}$, the room temperature $\boldsymbol{T}_{\mathrm{room},f}$ and the temperature band defined by the dashed lines, the cooling variable $\boldsymbol{\eta}_\mathrm{cool}$, and the cooling flow $\dot{\boldsymbol{Q}}_{\mathrm{cool},f}$ to the TABS.

An example for a possible scenario for a building MPC controlling TABS of floor f is shown in Fig. 7. The white rectangles denote the possible amount of cooling flow, due to the cooling variable η_cool, the rectangle inside denotes the applied cooling flow $\dot{\boldsymbol{Q}}_{\mathrm{cool},f} > 0$ to the TABS. The system acts before it violates the comfort temperature band and keeps on cooling to use the storage capacity of the building mass and the TABS to avoid a violation on the next day. This is only possible with a predictive control algorithm.

3.2. MMPC architecture

The input data vector to the MMPC is the vector $\boldsymbol{x}_\mathrm{measure}$, containing the room temperatures, the TABS temperatures and other states of the building service obtained by the measurement or observer-based reconstruction of actual values in the building. The set point temperatures $\boldsymbol{T}_\mathrm{set}$ for the TABS are its output. Furthermore, it is assumed that MMPC has predictions for weather and internal gain $\boldsymbol{z}_\mathrm{weather,gain}$. The structure of the MMPC is shown in Fig. 8 giving a detailed overview of the control loop. The MMPC controller is decomposed into three modules. An overview of the modules is given in this subsection. By decomposing the optimization problem several aims can be achieved: an efficient nonlinear controller is constructed that respects the switching behavior in the system, considers nonlinearities in the system dynamics and disturbance paths and is capable for real-time for future implementation in the building. The solution respects limited calculation capacities for building control. A similar hierarchically decoupled MPC problem for a different building is shown in [10].

The three modules of the MMPC are defined as follows:

Module 1: The input values $\boldsymbol{x}_{\mathrm{measure},k}$ measured on the building (temperatures, states of the building services model) are mapped to the vector $\boldsymbol{x}_{\mathrm{SBUI/SBS},k}$, which contains the initial values for the nonlinear model SBUI/SBS. Based on this input, SBUI/SBS generates the baseline trajectories $\widetilde{\boldsymbol{T}}_0 = [\boldsymbol{T}_{\mathrm{TABS},0}, \boldsymbol{T}_{\mathrm{room},0}, \boldsymbol{P}_{\mathrm{el},0}, \dot{\boldsymbol{Q}}_0]$, with the TABS temperatures $\boldsymbol{T}_{\mathrm{TABS},0}$, the room temperatures $\boldsymbol{T}_{\mathrm{room},0}$, the electric power $\boldsymbol{P}_{\mathrm{el},0}$ and the heat flows to the TABS $\dot{\boldsymbol{Q}}_0$. In this module of the MMPC, the predictions $\boldsymbol{z}_\mathrm{weather,gains}$ (weather and internal gains) affect the output. The output trajectory $\widetilde{\boldsymbol{T}}_0$ represents the nonlinear baseline disturbance response of the building.

Module 2: The goal of this module is to adjust the heat flows $\dot{\boldsymbol{Q}}$, while utilizing the baseline trajectories. More precisely, a linear discrete optimization problem is formulated using the linearized thermal dynamics state-space model described in Section 2.2.3. The input vector is equal to $\boldsymbol{u}_k = \boldsymbol{u}_{k,0} + \Delta\boldsymbol{u}_k$, and state vector is equal to $\boldsymbol{x}_k = \boldsymbol{x}_{k,0} + \Delta\boldsymbol{x}_k$, where $\boldsymbol{x}_{k,0}$ and $\boldsymbol{u}_{k,0}$ are given by the baseline

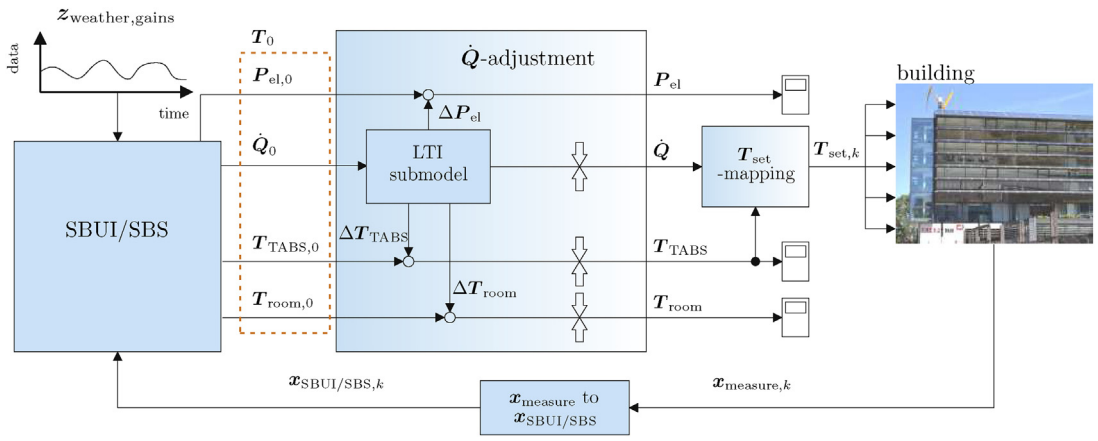

Fig. 8. Scheme for the MMPC with the simplified building/building service model SBUI/SBS, and the linear time invariant (LTI) submodel.

trajectories $\widetilde{\boldsymbol{T}}_0$ obtained in the first module. Vectors $\Delta\boldsymbol{x}_k$ and $\Delta\boldsymbol{u}_k$ satisfy the linearized thermal model equations (2). The constraints on the room and TABS temperatures ($\boldsymbol{T}_{\text{TABS}}$, $\boldsymbol{T}_{\text{room}}$) and the cost function also need to be formulated, represented by the arrows in Fig. 8. Module 2 produces vector $\boldsymbol{u}$ as output, i.e. the adjusted heat flows $\dot{\boldsymbol{Q}}$.

Module 3: (The $\boldsymbol{T}_{\text{set}}$-mapping) In this module, it is taken into account that the heat flows $\dot{\boldsymbol{Q}}$ can only be set to zero or state dependent heat flows (if the corresponding branch is open). The outputs of the $\boldsymbol{T}_{\text{set}}$-mapping are the set point trajectories $\boldsymbol{T}_{\text{set}}$ which realize an optimal actuation close to the desired heat flows $\dot{\boldsymbol{Q}}$ obtained in module 2. The values of the next time step $\boldsymbol{T}_{\text{set},k}$ are sent to the building.

3.3. Formulation of the optimization problems

This subsection describes the two consecutive optimization problems arising in the proposed MMPC concept: the $\dot{\boldsymbol{Q}}$-adjustment step (module 2) and the $\boldsymbol{T}_{\text{set}}$-mapping step (module 3).

3.3.1. Module 2 ($\dot{\boldsymbol{Q}}$-adjustment)

The $\dot{\boldsymbol{Q}}$-adjustment can be seen as main module of the MMPC and optimizes the desired heat flow trajectory $\dot{\boldsymbol{Q}}$. The optimization problem is formulated as

$$J(\boldsymbol{x}_k, \boldsymbol{u}_k) = \sum_{i=0}^{N_\text{p}-1} P_{\text{el},k+i} + \underbrace{\boldsymbol{w}^\text{T}\boldsymbol{s}}_{\text{violation penalty}} + \underbrace{\boldsymbol{w}_\text{mean}^\text{T}\boldsymbol{s}_\text{mean}}_{\text{deviation penalty}} \tag{11}$$

$$\boldsymbol{u}_k^* = arg \min_{\boldsymbol{u}_{k\ldots k+N_\text{p}-1}, \boldsymbol{s}, \boldsymbol{s}_\text{mean}} J(\boldsymbol{x}_k, \boldsymbol{u}_k) \tag{12}$$

$$\text{s.t.} \quad \boldsymbol{0} \le |\dot{\boldsymbol{Q}}_{0,k+i}| + \boldsymbol{u}_{k+i} \le |\dot{\boldsymbol{Q}}_{\max,k+i}| \quad \forall i = 0, \ldots, N_\text{p} - 1 \tag{13}$$

$$\boldsymbol{u}_{k+i} = \boldsymbol{0} \quad \text{if} \quad \eta_{k+i} = 0 \quad \forall i = 0, \ldots, N_\text{p} - 1 \tag{14}$$

$$\boldsymbol{1}^\text{T}\boldsymbol{u}_{\text{heat},k+i} \le \dot{Q}_{\text{sum,max}} \quad \forall i = 0, \ldots, N_\text{p} - 1 \tag{15}$$

$$T_{\min} - \boldsymbol{s} \le \boldsymbol{T}_{k+i} \le T_{\max} + \boldsymbol{s} \quad \forall i \in \boldsymbol{n}_{\text{office}} \tag{16}$$

$$T_{\text{room,set}} - \boldsymbol{s}_\text{mean} \le \bar{\boldsymbol{T}}_{\text{room}} \le T_{\text{room,set}} + \boldsymbol{s}_\text{mean}, \tag{17}$$

where

$$\boldsymbol{x}_k = \boldsymbol{x}_{k,0} + \Delta\boldsymbol{x}_k, \quad \boldsymbol{u}_k = \boldsymbol{u}_{k,0} + \Delta\boldsymbol{u}_k,$$

$$\Delta\boldsymbol{x}_{k+1} = \boldsymbol{A}\Delta\boldsymbol{x}_k + [\boldsymbol{B}, -\boldsymbol{B}]\Delta\boldsymbol{u}_k, \tag{18}$$

with $\boldsymbol{s} \ge 0$ the slack variables for the temperature band and $\boldsymbol{s}_\text{mean} \ge 0$ for the room reference temperature $T_{\text{room,set}}$, $\boldsymbol{w} = \boldsymbol{1} \cdot w$ the weights on the room and TABS temperature violations and $\boldsymbol{w}_\text{mean} = \boldsymbol{1} \cdot w_\text{mean}$ the weights on the violations of the mean temperatures, $\bar{\boldsymbol{T}}_{\text{room}}$ the mean room temperature during one office day, $\dot{\boldsymbol{Q}}_{\max,k+i}$ the maximal allowed heat flow at k and prediction step i and the maximal summed heat flow $\dot{Q}_{\text{sum,max}}$. $\boldsymbol{1}$ is a vector of ones with the same length as $\boldsymbol{u}_{\text{heat},k}$. $\boldsymbol{T}_{k+i}$ represents $\boldsymbol{T}_{\text{TABS},k+i}$ and $\boldsymbol{T}_{\text{room},k+i}$ being limited by the maximal and minimal temperatures $T_{\max}$ and $T_{\min}$. Note that the limits are different for room and TABS temperatures.

The linear cost function (11) consists of 3 parts: the summed-up electric energy, the penalties for temperature band violations, and the penalties for the mean room temperature deviations. At each prediction step, hard constraints are applied to the heating/cooling flows (13) and on the summed heat flows (15) being limited by the maximum heat flow achievable by the heat pumps. The soft constraints (16) are evaluated each full hour during office times 8:00–18:00, these sampling instances are collected in the set $\boldsymbol{n}_{\text{office}}$.

For feasibility reasons it is a common approach to soften the constraints of plants [30], especially for the temperature comfort band. Building MPC with soft constraints are also implemented in [3,18].

The mean constraint (17) serves two purposes: On the one hand it prevents $\boldsymbol{T}_{\text{room}}$ to stay on the lower or higher comfort limit as in [13,18], so that temperature violations due to prediction uncertainties are less likely. On the other hand it punishes the frequently observed MPC strategy to use existing heat energy in the TABS until the limit of the temperature band is reached, causing a "draining" trend in the temperature trajectories, which is not desired. Mean temperature constraints are simple to implement and their dedicated utilization represents a novel approach for predictive building control.

3.3.2. Solar tank energy

As an additional feature, the optimization problem takes into account that the solar energy stored in the solar tank can be used, by adding the following constraints to the optimization problem (11)–(16):

$$Q_{\text{solar,sum,disp},k+i} \ge Q_{\text{solar,sum,used},k+i} \quad \forall i = 0, \ldots, N_\text{p} - 1 \tag{19}$$

$$Q_{\text{solar,sum,used},k+i} = \sum_{l=k}^{k+i} (\dot{Q}_{\text{solar,used},l} \cdot T_\text{s}) \quad \forall i = 0, \ldots, N_\text{p} - 1 \tag{20}$$

$$\boldsymbol{1}^\text{T}\dot{\boldsymbol{Q}}_{\text{heat},k+i} \ge \dot{\boldsymbol{Q}}_{\text{solar,used},k+i} \quad \forall i = 0, \ldots, N_\text{p} - 1 \tag{21}$$

with $Q_{\text{solar,sum,disp},k+i}$, the disposable heat energy summed up until k, $Q_{\text{solar,sum,used},k+i}$, the used heat energy, $\dot{Q}_{\text{solar,used},k+i}$ the heat flow from the solar tank to the TABS. The optimization problem (12) contains the new decision variables $\dot{Q}_{\text{solar,used},k+i}$ which reduce $P_{\text{el},k+i}$

in the cost function (11). Note that in this case, additional states in (2) need to be introduced which contain the temperatures of the solar tank. For feasibility reasons, the constraint (19) is softened.

3.3.3. Module 3 ($\boldsymbol{T}_{set}$-mapping)

$\boldsymbol{T}_{\text{set}}$-mapping calculates $\boldsymbol{T}_{\text{set}}$ trajectories for CBUI/CBS. $\boldsymbol{T}_{\text{set}}$-mapping is a mixed-integer problem respecting the switching behavior of the supply system. The inlet temperature $T_{\text{in},k}$ is the same for all TABS, the optimal $\boldsymbol{T}_{\text{TABS}}$ trajectories are known from the $\dot{\boldsymbol{Q}}$-adjustment. The heat flow to the TABS in floor $f \in \{$ F0, F1, F23, F4$\}$ is defined by

$$\dot{\boldsymbol{Q}}_{\text{mi},k} = c_{\text{p}}\dot{\boldsymbol{m}}(T_{\text{in},k} - \boldsymbol{T}_{\text{TABS},f,k})^{\text{T}}, \tag{22}$$

with the specific heat capacity c_{p} and the constant mass flows $\dot{\boldsymbol{m}}$ to the TABS.

While in [14] a coupled problem is solved in one optimization step, in most of the existing publications switching inputs are not considered [13,15] or the building models are not detailed enough [3,7]. By setting $\boldsymbol{T}_{\text{in}}$ a priori, the mixed integer problem decouples and becomes efficiently solvable. The optimization problem is formulated as:

$$J_{\text{mi}}(u_{f,j,k}, \boldsymbol{x}_{f,j,k}) = \sum_{i=0}^{N_{\text{p,mi}}-1} \Delta_i \tag{23}$$

$$\dot{Q}^{*}_{\text{mi},f,j,k} = arg \min_{\boldsymbol{\Delta}\left(\dot{\boldsymbol{Q}}_{\text{mi},f,j}, \boldsymbol{n}_{\text{on/off}}\right)} J_{\text{mi}}(u_{f,j,k}, \boldsymbol{x}_{f,j,k}) \tag{24}$$

s.t. $\dot{Q}_{\text{mi},f,j,k+l} \in$

$$\begin{cases} 0, & \text{if} \quad \eta_{k+l} = 0 \\ 0, & \text{if} \quad n_{\text{on/off},k+l} = 0 \\ c_{\text{p}}\dot{m}_j(T_{\text{in},k+l} - T_{\text{TABS},f,j,k+l}), & \text{else} \quad \forall l = 0, \ldots, i \end{cases} \tag{25}$$

$$\Delta_i = \sum_{l=0}^{i} |\dot{Q}_{\text{mi},f,j,k+l} - \dot{Q}_{f,j,k+l}| T_{\text{s}} \quad \forall i = 0, \ldots, N_{\text{p,mi}} - 1, \tag{26}$$

with J_{mi} the cost function of the $\boldsymbol{T}_{\text{set}}$-mapping problem, $\Delta_i \geq 0$ the heat energy difference between the $\dot{\boldsymbol{Q}}$-adjustment solution $\dot{Q}_{j,k+l}$ and the $\boldsymbol{T}_{\text{set}}$-mapping solution $\dot{Q}_{\text{mi},j,k+l}$, $n_{\text{on/off},k+l} = \{0, 1\}$ representing a closed or open valve at prediction step $k+l$ and zone $j \in \{$N, S$\}$, the mixed integer prediction horizon $N_{\text{p,mi}} \leq N_{\text{p}}$ and $\dot{Q}^{*}_{\text{mi},j,k}$ the optimal solution over $N_{\text{p,mi}}$. Having obtained the optimal switching sequences $n_{\text{on/off},k+l}$ the setpoint temperatures are constructed so that the valve controllers inside the building services system safely produce the desired switching sequences.

Both problems, the $\dot{\boldsymbol{Q}}$-adjustment and the $\boldsymbol{T}_{\text{set}}$-mapping are formulated via the Yalmip toolbox [31]. $\dot{\boldsymbol{Q}}$-adjustment is solved with the solver `Linprog` [32] and $\boldsymbol{T}_{\text{set}}$-mapping with the `GNU linear programming kit` [33].

3.4. $\boldsymbol{T}_{set}$-update and move blocking

First simulations have shown that the sampling time of $T_{\text{s}} = 15$ min can be enlarged, without changing temperature band violations and electric consumption during the co-simulation, however significantly reducing calculation time. Two strategies are used for the simulation studies. $\boldsymbol{T}_{\text{set}}$ is updated each hour and a move blocking algorithm is implemented for the MMPC as in [14], so that $\boldsymbol{u}$ is changed every 30 min. Note that for feasibility reasons the input blocks have to be at the same points of time, moving forward with k, see [14].

3.5. Rule-based control

Rule Based Control is the current control strategy for the ENERGYbase. Depending on the measured ambient temperature T_{amb}, $\boldsymbol{T}_{\text{set}}$ is calculated. These dependencies are precise linear functions. They are different for heating and cooling and have been determined heuristically by expert knowledge. Whether heating or cooling windows of the RBC are activated depends on the ambient temperature. This approach is similar to using finite state machines, see [34,35].

4. Stability and robustness considerations

The proposed modular MPC inevitably faces model, prediction and measurement errors in operation (both in co-simulation with a complex building model as well as in subsequent realtime operation on the actual building). It is thus of interest to analyze, a posteriori, robust stability and performance in the presence of these errors, also because the proposed design procedure does not consider these errors a priori.

The considered building control loop (as depicted in Figs. 1 and 8) includes the highly complex nonlinear plant and the modular MPC with model-based modules. Being such a heterogeneous system, it cannot directly be characterized by rigorous standard tools of stability (or robust stability) analysis. In the following, one possible approach to conduct rigorous robust stability analysis on controllers involving a central linear MPC is sketched and discussed. However, both the required uncertainty modeling and the numeric analysis tasks require significant design, analysis, and computational effort which is out of scope of this work. For these reasons, the methodological discussion is kept at a qualitative level to highlight ways to adopt and utilize robust control methodologies in complex application problems such as the proposed building MMPC, and empirical co-simulation-based validation studies are carried out to validate stability, performance, and robustness in Section 5.

4.1. Robustness analysis centered on LTI MPC (module 2)

The MMPC-controlled building control loop is viewed from the linearization view of module 2: driven by nonzero initial conditions, the analysis task can be formulated as the stabilization of the linearized thermal plant with module 2's MPC law and subject to uncertainties and disturbances. To formulate an appropriate robust control system structure and appropriate, well-known types of uncertainty models [36] for the problem, the following system aspects are of special interest:

- The model errors between the complex model (CBUI/CBS), the simplified nonlinear prediction model (SBUI/SBS) and the linearized thermal dynamics, as well as the deviations arising from the imperfect realization of the demanded TABS heat flows via the switching valves distribution architecture need to be mapped to suitable uncertainty models.
- The switching behavior of the two-point relay control loops of each switching TABS feed line is smoothed by the large TABS' thermal capacitances. Note that uncertainties in switching times between modeled and actual plant dynamics produce a discontinuous heat flow error, however, its integral effect on the thermal states (or on the consumed energy) is continuous.
- The transfer from heat flow $\dot{Q}$ to TABS temperature T_{TABS} exhibits PT1-behavior. An uncertain actuated heat flow can be modeled by a multiplicative input uncertainty; uncertainty in the capacitance affect the PT1 pole position (which may be modeled by a parametric uncertainty of the system matrix).

- Uncertain cross-coupling between thermal zones can be represented, for example, by an additive uncertainty.
- Uncertain or unknown disturbance effects and gains act only in a feed-forward fashion, so they are considered irrelevant for stability studies. They, however, do affect performance and require closed-loop validation of control performance.

All these uncertain blocks can in principle be generated from extensive co-simulation studies and/or bounded using expert knowledge.

4.2. Robust stability test via piecewise Lyapunov functions in the TS-fuzzy framework

Let the LTI MPC act in feedback loop with its LTI design plant of the simplified thermal building dynamics, and all deviations to these perfect dynamics be modeled by a suitable uncertainty model. Together with the MPC law's structure, this uncertainty model needs to efficiently cover the actual model errors, be quantifiable via expert knowledge and co-simulations, and allow a tractable robustness analysis. Note that a successful robustness analysis depends on the mathematical problem structure of the LTI MPC problem and the availability of effective analysis tools. One possible conceptual path towards such analysis is sketched as follows:

- Express the proposed LTI MPC law (linear objective, linear constraints) as piecewise-affine (PWA) function of time and state, i.e. as an explicit MPC law.
- Formulate the uncertain LTI system dynamics covering the observed relevant model errors by a structured polytopic uncertainty description.
- Construct the feedback interconnection of the uncertain plant model and the PWA explicit MPC law, resulting in uncertain piecewise-affine closed-loop system dynamics.
- Analyze robust stability and performance for the closed loop via LMI methods available for uncertain TS-fuzzy system analysis [37]. Note that uncertain PWA dynamics is a special case of uncertain TS-fuzzy system dynamics.

To formalize this conceptual path, the LTI-MPC control law is considered in an explicit form as a piecewise-affine (PWA) function:

$$\boldsymbol{u}_k = \boldsymbol{K}_l \boldsymbol{x}_k + \boldsymbol{z}_l, \quad \boldsymbol{x}_k \in \mathcal{X}_l, \quad l \in L \tag{27}$$

where it is assumed that $\mathcal{X}_l$ is a bounded polyhedral partitioning of the (bounded) set of admissible states $\mathbb{X} = \bigcup_{l \in L} \mathcal{X}_l$ and $\boldsymbol{z}_l$ denotes an affine term possibly including nonzero constant reference input terms.

It is furthermore assumed that the linearized thermal system behaviour can be described by LTI system dynamics subject to bounded uncertainties in the parameters of the form

$$\boldsymbol{x}_{k+1} = \left(\boldsymbol{A} + \boldsymbol{\Delta_A}\right) \boldsymbol{x}_k + \left(\boldsymbol{B} + \boldsymbol{\Delta_B}\right) \boldsymbol{u}_k. \tag{28}$$

Then, substituting (27) into (28) yields an uncertain PWA system

$$\boldsymbol{x}_{k+1} = \left(\widetilde{\boldsymbol{A}_l} + \widetilde{\boldsymbol{\Delta}_{A_l}}\right) \boldsymbol{x}_k + \left(\boldsymbol{B} + \boldsymbol{\Delta_B}\right) \boldsymbol{z}_l \tag{29}$$

with

$$\widetilde{\boldsymbol{A}_l} = \boldsymbol{A} + \boldsymbol{B}\boldsymbol{K}_i$$

$$\widetilde{\boldsymbol{\Delta}_{A_l}} = \boldsymbol{\Delta_A} + \boldsymbol{\Delta_B}\boldsymbol{K_l}, \quad l \in L.$$

It is noted that these generic uncertainties are bounded in the form $\widetilde{\boldsymbol{\Delta}_{A_l}}^{\mathrm{T}} \widetilde{\boldsymbol{\Delta}_{A_l}} \leq \boldsymbol{E}_{lA}^{\mathrm{T}} \boldsymbol{E}_{lA}$, and methods to compute these bounds are outlined in [38–40].

Verifying that the uncertain PWA system (29) is robustly stable for all admissible instances of the uncertainties can be done by understanding (29) as a special case of an uncertain TS-fuzzy system and verifying Lyapunov stability using the common quadratic, piecewise quadratic or fuzzy Lyapunov function methods [37]. As an example, the well-known stability argument using piecewise-quadratic Lyapunov functions, taken from Theorem 4.2 in [37] is adapted to test robust stability for the considered closed-loop system:

Definition 1. The set Ω of possible transitions among regions is defined as

$$\Omega = \Big\{ (j,k) | j \neq k, \exists \boldsymbol{x} \in \mathcal{X}_j, \widetilde{\boldsymbol{D}_A} \in \widetilde{\boldsymbol{\Delta}_{A_j}}, \widetilde{\boldsymbol{D}_B} \in \boldsymbol{\Delta_B} : \left(\widetilde{\boldsymbol{A}_j} + \widetilde{\boldsymbol{D}_A}\right) \boldsymbol{x} + \left(\boldsymbol{B} + \widetilde{\boldsymbol{D}_B}\right) \boldsymbol{z}_j \in \mathcal{X}_k \Big\}.$$

Theorem 1 (adopted from Theorem 4.2 in [37]). *Given a PWA function (27) with $\boldsymbol{z}_l \equiv \boldsymbol{0}$, uncertain system (28) with state partitioning $\mathcal{X}_l, l \in L$, uncertainty bounds $\boldsymbol{E}_{lA} : \widetilde{\boldsymbol{A}_l}^{\mathrm{T}} \widetilde{\boldsymbol{A}_l} \leq \boldsymbol{E}_{lA}^{\mathrm{T}} \boldsymbol{E}_{lA}$ and the set of possible transitions Ω, the uncertain closed-loop system is robustly and globally exponentially stable if there exists a set of symmetric positive definite matrices $\boldsymbol{P}_l$, $l \in L$ such that the following linear matrix inequalities are satisfied,*

$$\begin{bmatrix} \boldsymbol{A}_l^{\mathrm{T}} \boldsymbol{P}_l \boldsymbol{A}_l - \boldsymbol{P}_l + \boldsymbol{E}_{lA}^{\mathrm{T}} \boldsymbol{E}_{lA} & \boldsymbol{A}_l^{\mathrm{T}} \boldsymbol{P}_l \\ \boldsymbol{P}_l \boldsymbol{A}_l & -(\mathbf{I} - \boldsymbol{P}_l) \end{bmatrix} < 0, \qquad l \in L \tag{30}$$

$$\begin{bmatrix} \boldsymbol{A}_l^{\mathrm{T}} \boldsymbol{P}_j \boldsymbol{A}_l - \boldsymbol{P}_l + \boldsymbol{E}_{lA}^{\mathrm{T}} \boldsymbol{E}_{lA} & \boldsymbol{A}_l^{\mathrm{T}} \boldsymbol{P}_j \\ \boldsymbol{P}_j \boldsymbol{A}_l & -\left(\mathbf{I} - \boldsymbol{P}_j\right) \end{bmatrix} < 0, \qquad (l,j) \in \Omega. \tag{31}$$

Proof 1. The proof is equivalent to the proof of Theorem 4.2 in [37] (pp.60–62).□

It is noted that representing a complex MPC law in the explicit PWA form (27) can produce a prohibitively high number of regions, so that the robust stability proof becomes intractable or even the explicit MPC characterization infeasible. Methods to reduce the region count exist that could resolve this difficulty, however this task is out of scope of this work.

Instead, a range of numeric results based on empirical robustness and performance co-simulation studies will be given in the next section. From these results it will become clearly evident that the proposed scheme provides high control performance and is robust to relevant uncertainties in prediction and model errors.

5. Results

In this chapter the model validation, the model errors, a co-simulation study and tuning possibilities are presented. The results demonstrate the high control performance and indicate the robustness of the controller with respect to prediction uncertainties of weather and internal gains.

5.1. Co-simulation

For the co-simulation studies, the real building is replaced by CBUI/CBS. Both CBUI/CBS and SBUI/SBS are modeled in Modelica. The co-simulation uses MATLAB as master and accesses the Modelica models during the co-simulation.

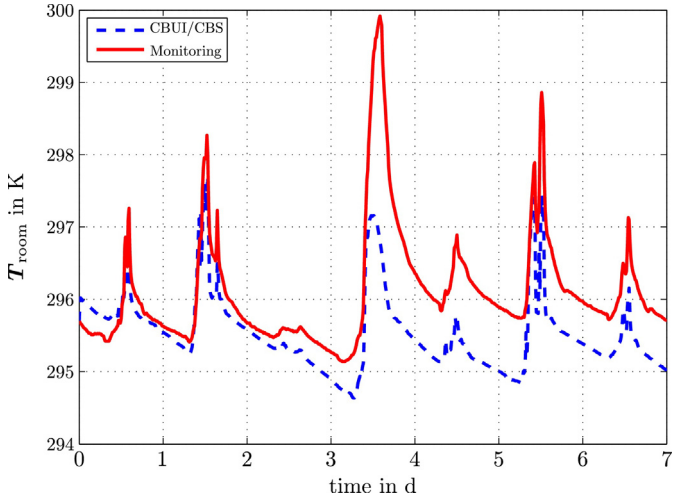

Fig. 9. CBUI/CBS (complex building model/building system) – monitoring data, validation of the room temperature for a reference zone, taken from [26].

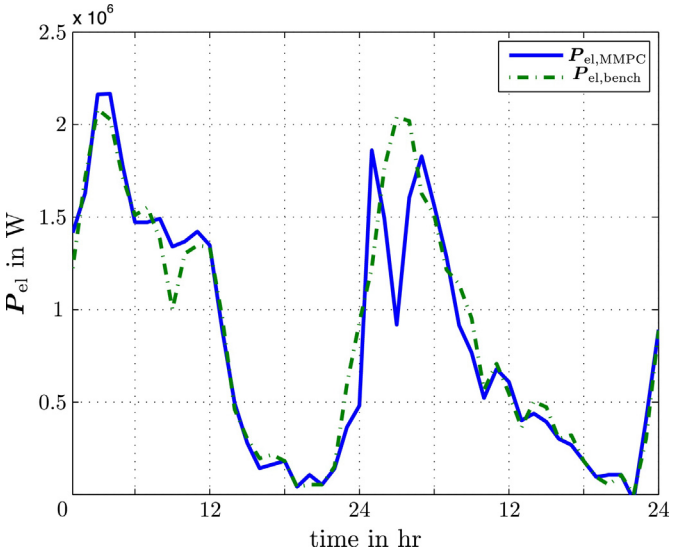

Fig. 11. Comparison of the predicted electric consumption $\boldsymbol{P}_{el}$ between the benchmark (bench) results and the results of the modular model predictive controller (MMPC).

5.2. Model validation

CBUI/CBS is compared with monitoring data and with SBUI/SBS. The two relevant model errors concerning the white box models are:

1 CBUI/CBS vs. monitoring data: Fig. 9 shows the validation results of a reference zone against monitoring data. The zone is not influenced by internal gains. The overall dynamic shows a reasonable fit. Towards the end of the simulation, a deviation between model and monitoring data occurs due to simplifications in boundary conditions to the adjacent zones and floors. The residual sum of squares (*RSS*) between $\boldsymbol{T}_{room}$ of the real building and CBUI divided by the number of samples $n_{samples}$ is $RSS/n_{samples} = 0.6242\ K^2$.
2 CBUI/CBS vs. SBUI/SBS: Fig. 10(a) shows a comparison of the electric energy demand of the heat pumps for two days in January between CBS and SBS. The figure displays a good match in terms of the dynamic behavior of the system. The deviation regarding the absolute value arises due to the simplification of the zones and, the overall consumption of E_{el} differs by 9% after 48 h. Fig. 10(b) compares the room temperature profiles between CBUI and SBUI. It shows the temperature behavior of two room zones of CBUI summed up to the SE room zone in SBUI. The zone of SBUI stays in 85% of the sampling steps inside zone 1 and zone 2 of CBUI, violating this area by a maximum of $\Delta T_{viol} = 0.07$ K.

The match of the two models and CBUI/CBS with the measured data is satisfying and it is seen justified that the models can be used for building control.

5.3. Linearization error

The linearization error is produced because the $\dot{\boldsymbol{Q}}$-adjustment-module of the MMPC solves an approximated linearized problem. The error of the MMPC is calculated by comparing E_{el} and $\boldsymbol{T}_{room}$ between the prediction of the MMPC and the prediction of a benchmark run of SBUI/SBS using $\boldsymbol{T}_{set}$ of the MMPC result.

The 2-day co-simulation scenario uses the prediction data from 2011-02-14 to 2011-02-17. The benchmark simulation of SBUI/SBS is calculated with the determined $\boldsymbol{T}_{set}$ from the MMPC at the same simulation step for $N_{p,mi} = 6$ h resulting in $\boldsymbol{y}_{bench}$.

The comparison of $\boldsymbol{P}_{el}$ at each co-simulation step for $N_{p,mi} = 6$ h is shown in Fig. 11. The overall predicted energy consumption for this co-simulation run differs by 3%. The *RSS* between $\boldsymbol{T}_{room,bench}$ and $\boldsymbol{T}_{room,MMPC}$ divided by $n_{samples}$ is $RSS/n_{samples} = 0.0146\ K^2$. The maximal deviation is $|\Delta T_{room,alg,max}| = 1.644$ K. These are considered acceptable errors, resulting in a good match between the MMPC and SBUI/SBS.

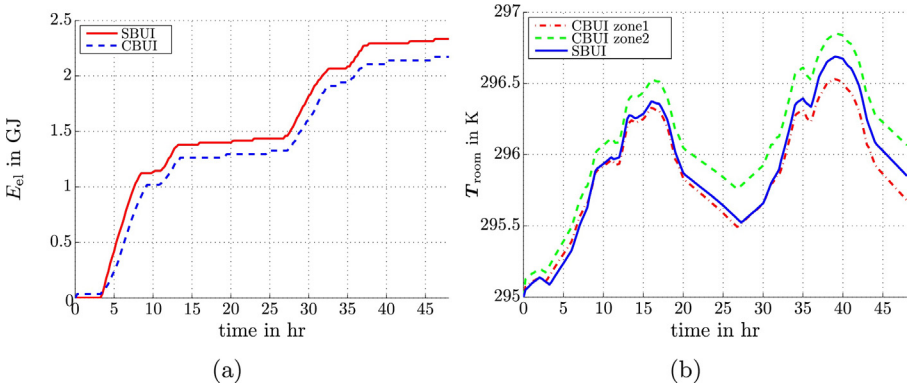

Fig. 10. CBUI/CBS – SBUI/SBS (complex – simplified building model/building system), (a) results of the electricity demand of the heat pumps and (b) results of the room temperatures, compare [26].

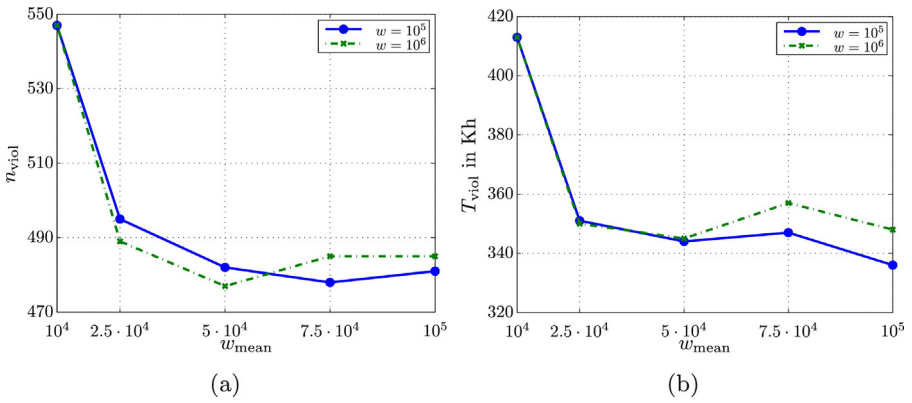

Fig. 12. T_{viol} and n_{viol}, the temperature band violations for the temperature band constraint and weights $w = 10^5$ and $w = 10^6$.

5.4. Simulations

Although the robustness analysis of the MMPC control system has not been done in this paper, in this subsection the robustness to disturbance and model uncertainties is observed in the simulations.

For the co-simulation studies five scenarios are considered: S1 uses perfect prediction data, S2–S5 address the prediction uncertainties of weather and internal gains:

S5 utilizes the predicted weather data for 3 days. The MMPC receives the prediction data for the third day, while the CBUI/CBS uses the predictions of the first day. Additionally, the internal gain data of CBUI/CBS is halved for SBUI/SBS. The simulation duration is 7 days beginning at 2014-07-24.

S1–S4 use weather data of 2011 and available internal gain data of 2013 for prediction and disturbance. The simulations take place in the first week of April, where both heating and cooling is necessary. The internal gain predictions and the weather predictions of S2 are varying by up to ±30%. Two times the weather prediction error of S5 is used to modify the weather predictions of S3, and the internal gains are decreased by 30%. S4 uses the same weather prediction data as S3 but, contrary to S3, the internal gains are increased by 30%.

5.4.1. MMPC tuning — mean constraint

The effect of the mean constraint on the robustness of the MMPC to weather and internal gain uncertainties is observed in this subsection. Scenario S5 is used to tune the mean constraint weighting w_{mean} from (11). The violations of the temperature band T_{viol} in Kelvin·hours and the number of temperature violations per hour n_{viol} are used to evaluate the room comfort, both are summed up over the simulation horizon. Due to the results in Fig. 12, $w_{mean} \geq 2.5 \times 10^4$ should be chosen. For weights higher than $w_{mean} = 2.5 \times 10^4$, no improvement of the room comfort can be seen in the simulation. The result does not depend on w for the two simulated variants $w = 10^5$ and $w = 10^6$.

5.4.2. Robustness to disturbance uncertainties

Fig. 13 demonstrates the robustness of the MMPC algorithm concerning prediction uncertainties, because S2, S3 and S4 lie very close to the scenario S1 with ideal prediction data.

Simulations using the scenarios S1–S4 are performed in this section. Each of the scenarios is simulated with varying weighting $w \in \{7.5 \times 10^3, 10^4, 5 \times 10^4, 10^5, 5 \times 10^5, 10^6\}$ with a fixed weighting ratio of $r = w_{mean}/w = 0.5$. The results in Fig. 13 show the trade-off between the consumption of E_{el} and the amount of the temperature band violations T_{viol} in Kh per simulation period.

Fig. 13 shows the result of the co-simulations. Next to each of the simulation results the utilized weighting w is noted. S1 is considered to form the optimal discrete Pareto front represented by the dash-dotted line in Fig. 13. The results of the scenarios S2, S3 and S4 are located above the discrete Pareto front due to the prediction errors. Note that violations of the discrete two-dimensional Pareto front might be possible, because the mean constraint in the cost function (11) is not evaluated in the plot. The results of S2 compared to S3 show that the prediction data of S3 is more challenging for the MMPC. The result of S4 with $w = 10^5$ indicates that overestimating the internal gains has the same effect as underestimation.

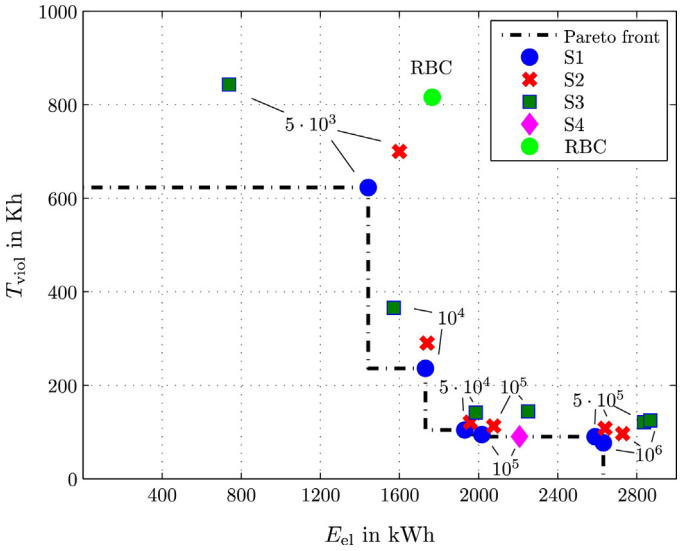

Fig. 13. Simulation results of scenarios S1, S2, S3, S4 and result of the Rule-Based Control (RBC) algorithm. The dash-dotted line illustrates the discrete Pareto front formed by S1. The numbers denote the weighting of the temperature band constraint w.

Since S2, S3 and S4 are close to S1, the MMPC is clearly robust to weather and internal gain prediction uncertainties.

Fig. 14 shows the capability of the MMPC to control heating and cooling of the building simultaneously. For S1 and $w = 5 \times 10^5$, the temperature trajectories $\boldsymbol{T}_{room,F3}$ and $\boldsymbol{T}_{TABS,F3}$ and the overall thermal flow $\dot{\boldsymbol{Q}}_{sum} = [\dot{Q}_{heat,sum}, \dot{Q}_{cool,sum}]$ for heating and cooling of the building is shown.

5.4.3. Robustness to model uncertainties

Next, the robustness of the MMPC with respect to building model uncertainties is observed. Three different cases have been simulated. In scenario S1 it is assumed that the concrete capacities of the building model are correct. In scenarios S2 and S3, the concrete capacities of the building model are 20% higher and 20% lower than the ones of the building, respectively. The simulation results

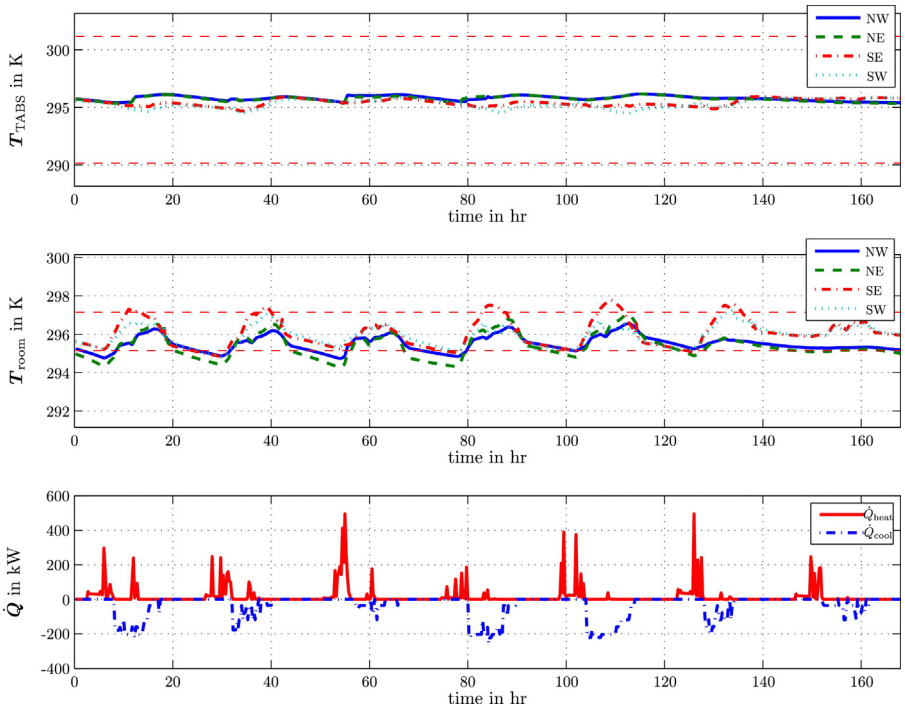

Fig. 14. Temperature trajectories and the overall heat flow using the weather prediction data from 2011-04-01 to 2011-04-07.

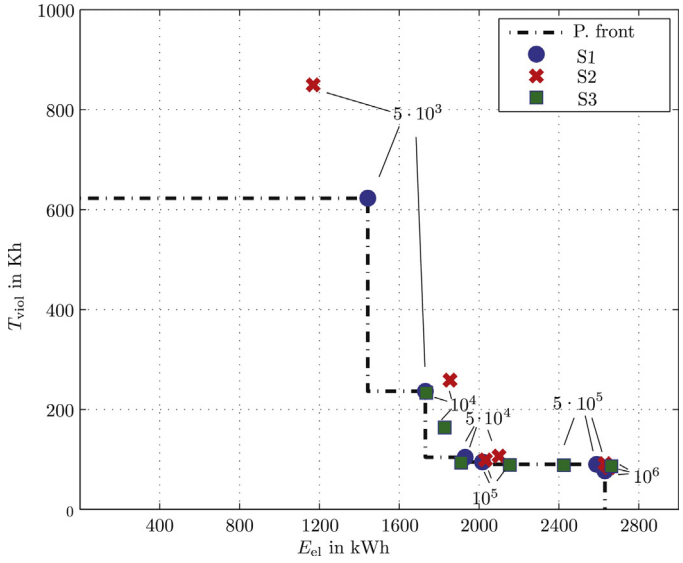

Fig. 15. Simulation results of scenarios S1, S2, S3. The dash-dotted line represents the discrete Pareto front formed by S1. The results are obtained for different weights of the temperature band constraint w, which are specified in the plot.

for the first week of April are plotted in Fig. 15. The results for the scenarios S2 and S3 stay very close to the optimal discrete Pareto front, which indicates that MMPC is robust to model uncertainties as well.

6. Conclusions

This paper introduces a new variant of a nonlinear building MPC for TABS, that is built in a modular structure and considers a nonlinear, white-box plant model. The simulation results for the MMPC show the robustness to prediction uncertainties (weather and internal gains). The robustifying effect of mean constraints on prediction uncertainties is analyzed.

The modular concept of the MMPC allows to use a highly detailed building model based on plan data, but at the same time, it keeps the calculation time low with a factor of $f = 15$ under real time. Although using a modular concept, the linearization error done by solving a linear optimization problem in a module of the MMPC remains small, as shown in Section 5.3. Mixed integer programming for building MPC is found in a few other publications such as [14], but the modular concept is novel for building MPC applications.

Furthermore, using the proposed weighting of the mean constraint reduces the temperature violations and makes the MMPC more robust to change of predictions as observed in Fig. 13. Also the tuning possibilities of the MMPC between room comfort violations and consumption of electric energy are demonstrated. MMPC shows higher performance over a traditional Rule based control scheme. The RBC is compared against a discrete Pareto front obtained by the MMPC simulation results, and it is seen that MMPC is able to reduce energy consumption while achieving smaller violation of the comfort band. As shown in Fig. 14, the MMPC is capable of simultaneously controlling heating and cooling of the system.

Follow-up simulation studies could be extended to utilize ventilation coils in the rooms. Additionally, with only minimal changes in the algorithm, the provided electric energy produced by a photovoltaic system as well as dynamic pricing can be considered. The capabilities of the controller in a real-world hardware-in-the-loop setting will be investigated on the ENERGYbase.

Acknowledgements

This work is a part of the SmartCityGrid: CoOpt project. The Climate and Energy Fund (“Klima- und Energiefonds KLIEN”) operated by the Austrian Research Promotion Agency (FFG) is gratefully acknowledged for their financial support of the SmartCityGrid: CoOpt project in the funding program “Neue Energien 2020” No. 834677.

References

[1] J. Laustsen, Energy Efficiency Requirements in Building Codes, Energy Efficiency Policies for New Buildings, International Energy Agency (IEA), 2008, pp. 477–488.
[2] EUROPEAN COMMISSION, GREEN PAPER Towards a European Strategy for the Security of Energy Supply, Office for Official Publications of the European Communities, Luxembourg, 2001.
[3] J. Široký, F. Oldewurtel, J. Cigler, S. Prívara, Experimental analysis of model predictive control for an energy efficient building heating system, Appl. Energy 88 (9) (2011) 3079–3087.
[4] A. Afram, F. Janabi-Sharifi, Theory and applications of HVAC control systems – a review of model predictive control (MPC), Build. Environ. 72 (2014) 343–355.
[5] B. Mayer, M. Killian, M. Kozek, Management of hybrid energy supply systems in buildings using mixed-integer model predictive control, Energy Convers. Manag. 98 (2015) 470–483.
[6] S. Prívara, J. Cigler, Z. Váňa, F. Oldewurtel, C. Sagerschnig, E. Žáčeková, Building modeling as a crucial part for building predictive control, Energy Build. 56 (2013) 8–22.
[7] S. Prívara, J. Široký, L. Ferkl, J. Cigler, Model predictive control of a building heating system: the first experience, Energy Build. 43 (2) (2011) 564–572.
[8] M. Castilla, J. Álvarez, M. Berenguel, F. Rodríguez, J. Guzmán, M. Pérez, A comparison of thermal comfort predictive control strategies, Energy Build. 43 (10) (2011) 2737–2746.
[9] R.Z. Freire, G.H. Oliveira, N. Mendes, Predictive controllers for thermal comfort optimization and energy savings, Energy Build. 40 (7) (2008) 1353–1365.
[10] B. Mayer, M. Killian, M. Kozek, Cooperative and hierarchical fuzzy MPC for building heating control, in: International Conference on Fuzzy Systems (FUZZ-IEEE), IEEE, 2014, pp. 1054–1059.
[11] S.C. Bengea, A.D. Kelman, F. Borrelli, R. Taylor, S. Narayanan, Model predictive control for mid-size commercial building HVAC: implementation, results and energy savings, in: The Second International Conference on Building Energy and Environment, 2012.
[12] I. Hazyuk, C. Ghiaus, D. Penhouet, Optimal temperature control of intermittently heated buildings using model predictive control: Part I – Building modeling, Build. Environ. 51 (2012) 379–387.
[13] I. Hazyuk, C. Ghiaus, D. Penhouet, Optimal temperature control of intermittently heated buildings using model predictive control: Part II – Control algorithm, Build. Environ. 51 (2012) 388–394.
[14] Y. Ma, F. Borrelli, B. Hencey, B. Coffey, S. Bengea, P. Haves, Model predictive control for the operation of building cooling systems, IEEE Trans. Control Syst. Technol. 20 (3) (2012) 796–803.
[15] F. Oldewurtel, A. Parisio, C.N. Jones, D. Gyalistras, M. Gwerder, V. Stauch, B. Lehmann, M. Morari, Use of model predictive control and weather forecasts for energy efficient building climate control, Energy Build. 45 (2012) 15–27.
[16] M. Morari, M. Baotic, F. Borrelli, Hybrid systems modeling and control, Eur. J. Control 9 (2) (2003) 177–189.
[17] A. Kelman, Y. Ma, F. Borrelli, Analysis of local optima in predictive control for energy efficient buildings, J. Build. Perform. Simul. 6 (3) (2013) 236–255.
[18] Y. Ma, A. Kelman, A. Daly, F. Borrelli, Predictive control for energy efficient buildings with thermal storage, IEEE Control Syst. Mag. 32 (1) (2012) 44–64.
[19] J.E. Braun, Load control using building thermal mass, J. Solar Energy Eng. 125 (3) (2003) 292–301.
[20] F. Oldewurtel, D. Sturzenegger, M. Morari, Importance of occupancy information for building climate control, Appl. Energy 101 (2013) 521–532.
[21] F. Oldewurtel, A. Parisio, C.N. Jones, M. Morari, D. Gyalistras, M. Gwerder, V. Stauch, B. Lehmann, K. Wirth, Energy efficient building climate control using stochastic model predictive control and weather predictions, in: American Control Conference (ACC), IEEE, 2010, pp. 5100–5105.
[22] X. Zhang, G. Schildbach, D. Sturzenegger, M. Morari, Scenario-based MPC for energy-efficient building climate control under weather and occupancy uncertainty, in: European Control Conference (ECC), IEEE, 2013, pp. 1029–1034.
[23] S. Koehler, F. Borrelli, Building temperature distributed control via explicit MPC and "Trim and Respond" methods, European Control Conference (ECC), IEEE, 2013, pp. 4334–4339.
[24] C. Ghiaus, I. Hazyuk, Calculation of optimal thermal load of intermittently heated buildings, Energy Build. 42 (8) (2010) 1248–1258.
[25] ENERGYbase: Concept, 2016 https://viennabusinessagency.at/property/project-development/energybase/ (accessed 10.05.16).
[26] T. Ferhatbegovic, S. Hauer, I. Leobner, K. Ponweiser, A. Schirrer, M. Kozek, Thermal building modeling and simulation for automated load shifting purposes in the non-residential building sector, in: Proceedings of the 10th European Conference on Product and Process Modelling, ECPPM, 2014, pp. 511–516.
[27] VDI, 6020: Anforderung an Rechenverfahren zur Gebäude- und Anlagensimulation, VDI, Düsseldorf, Beuth-Verlag, Berlin, 2001.
[28] M. Brandstetter, A. Schirrer, M. Miletic, S. Henein, M. Kozek, F. Kupzog, Hierarchical predictive load control in smart grids, IEEE Trans. Smart Grid (2016), http://dx.doi.org/10.1109/TSG.2015.2477105, in press.
[29] S. Yuan, R. Perez, Multiple-zone ventilation and temperature control of a single-duct VAV system using model predictive strategy, Energy Build. 38 (10) (2006) 1248–1261.
[30] E.C. Kerrigan, J.M. Maciejowski, Soft constraints and exact penalty functions in model predictive control, in: Control 2000 Conference, Cambridge, 2000.
[31] J. Loefberg, YALMIP: a toolbox for modeling and optimization in MATLAB, in: International Symposium on Computer Aided Control Systems Design, IEEE, 2004, pp. 284–289.
[32] G.B. Dantzig, A. Orden, P. Wolfe, et al., The generalized simplex method for minimizing a linear form under linear inequality restraints, Pac. J. Math. 5 (2) (1955) 183–195.
[33] GNU Linear Programming Kit, Version 4.48, 2014 http://www.gnu.org/software/glpk/glpk.html (accessed 29.09.14).
[34] F. Wagner, R. Schmuki, T. Wagner, P. Wolstenholme, Modeling Software with Finite State Machines: A Practical Approach, CRC Press, 2006.
[35] T.S. Chow, Testing software design modeled by finite-state machines, IEEE Trans. Softw. Eng. 4 (3) (1978) 178–187.
[36] S. Skogestad, I. Postlethwaite, Multivariable Feedback Control: Analysis and Design, vol. 2, Wiley New York, 2007.
[37] G. Feng, Analysis and Synthesis of Fuzzy Control Systems: a model-based approach, Vol. 37, CRC press, 2010.
[38] S.-G. Cao, N.W. Rees, G. Feng, Stability analysis of fuzzy control systems, IEEE Trans. Syst. Man Cybern. 26 (1) (1995) 201–204.
[39] S. Cao, N. Rees, G. Feng, Stability analysis and design for a class of continuous-time fuzzy control systems, Int. J. Control 64 (6) (1996) 1069–1087.
[40] S.-G. Cao, N.W. Rees, G. Feng, Analysis and design for a class of complex control systems. Part II: Fuzzy controller design, Automatica 33 (6) (1997) 1029–1039.